Linear Fabry-Perot/Leaky Wave Antennas Excited by Multiple Sources

Filippo Costa, *Member, IEEE*, Davide Bianchi, *Member, IEEE*, Agostino Monorchio, *Fellow, IEEE*, Giuliano Manara, *Fellow, IEEE*

***Abstract*— Fabry-Perot/Leaky Wave antennas fed with multiple sources are analyzed and modelled. A transmission line approach for a rapid and efficient analysis of such antenna configuration is developed. The method is based on the superposition of the travelling leaky waves excited by each of the applied sources. The field distribution inside the cavity is derived by using a longitudinal transmission line model which takes into account the interference of the multiple leaky waves excited by the sources. The radiation pattern of the multiple fed antenna is obtained by using the Fast Fourier transformation of the field distribution. The propagation constants of the leaky waves, travelling inside the Fabry-Perot cavity, are computed analytically and the accuracy of the proposed expressions is verified by using the Transverse Resonance Method (TRM) approach. A novel and accurate closed form expression for the leaky wave propagation constant has been derived. A detailed analysis of the antenna properties is carried out by using the model showing how this antenna configuration is suitable for designing very large aperture antennas with very high gain and fairly acceptable bandwidth. A prototype of a multi-feed Fabry-Perot antenna has been fabricated by using 3D printing technology and tested.**

***Index Terms*— Array, Fabry-Perot antennas, Leaky wave antennas, Frequency Selective Surfaces (FSS), Metamaterials, Overlapped Arrays.**

I. INTRODUCTION

Leaky antennas are designed by suitably controlling the leakage rate of a guiding structure [1]. This is achieved by properly modifying the geometry of the guiding structure. There exists a number of possibilities to achieve the desired goal and they mainly depend on the type of mode propagating inside the guiding structure [1]. One example of leaky antenna consists of a Partially Reflecting Surface (PRS) located half-wavelength apart from an electric ground plane. If the PRS is replaced by a perfect electric surface, the guiding structure is basically a parallel plate waveguide supporting the fundamental mode and two higher order modes (TE1 and TM1). The PRS is used to induce the modes to gradually radiate the travelling energy.

The antenna is usually fed at the center to synthesize a fan beam formed by the interference of the two leaky waves travelling towards opposite directions [2]. This antenna is frequently interpreted as a Fabry-Perot cavity by using ray optics [3]–[5]: in this case the leaky waves are represented by the rays bouncing from the top and to bottom of the cavity and vice versa, gradually releasing in-phase electric fields.

A typical problem of these antennas is the limited operating bandwidth since the resonance condition is achieved only for a single frequency [4]. The quality factor of the antenna is directly proportional to the reflectivity of the PRS surface, i.e. the higher is the PRS reflectivity, the higher is the peak gain but the narrower is the operating bandwidth [6]. Indeed, when the PRS reflectivity is increased, the guided wave is released more slowly as a function of distance from the source. If one needs to use a leaky antenna in place of a very large antenna array, a low leakage rate has to be selected to spread the energy along the cavity, but this clearly determines a very narrow operating bandwidth.

There exist different techniques to increase the operating bandwidth and most of them operate on the PRS superstrate to modify its phase response for having a positive gradient and thus guaranteeing the resonance condition of the guiding structure at multiple frequencies [7], [8]. This solution is effective for enlarging the bandwidth, but it leads to an increase of the total thickness of the antenna. More importantly, it does not allow controlling the amplitude of the reflection coefficient of the PRS independently of the phase response. This implies that it is not possible to choose the leakage rate and thus select arbitrarily the aperture illumination and the antenna gain [9].

An approach to design a very high gain leaky antenna is to feed it with multiple sources [10]–[15]. Multi-feed Fabry-Perot (FP) antennas have been also proposed for reducing the peak sidelobe level of arrays [16] or to perform a limited scan of the beam by changing the element phases [12].Multi-feed leaky antennas do not need unconventional superstrates as in the case of wideband FP antenna but a standard inductive or capacitive FSS can be employed [17], [18]. This is a great advantage in terms of analysis since the grid superstrate can be treated analytically in terms of surface impedance by homogenization theory. The reflectivity of the PRS can be modified to select the appropriate leakage rate. Choosing a moderately high leakage rate guarantees a reasonable bandwidth if a suitable number of feeds is selected to efficiently illuminate an arbitrary large area. The design is usually performed by using a full-wave approach, but this can be very expensive from a computational point of view.

Here a transmission line approach to analyze one-dimensional multi-feed leaky antennas is proposed. The method allows easily

Manuscript received December 30th, 2016.

F. Costa, D. Bianchi, A. Monorchio, G. Manara are with the Microwave and Radiation Laboratory at the Department of Information Engineering, University of Pisa, 56122 Pisa, Italy.

controlling the high number of degrees of freedom involved in the antenna design and thus optimizing its performance. The paper is organized as follows. In section II the analyzed structure is introduced. Section III is focused on the leaky analysis of the antenna where a novel accurate analytical expression of the leaky constant is derived. In section IV the longitudinal transmission line model to analyze the multi-feed leaky antenna is derived. Section V reports several numerical results on a benchmark antenna configuration for validating the accuracy of the analytical tool and to discuss the properties of the antenna. Section VI is dedicated to a discussion of the most relevant parameters involved in the design of multi-feed leaky antennas. In section VII a large aperture antenna configuration is presented. Finally, conclusions are drawn in Section VIII.

II. Structure under analysis

The analyzed leaky antenna configuration is composed by a one-dimensional shielded Fabry-Perot cavity excited by multiples waveguides. The cavity comprises a metallic waveguide whose top face is replaced with a PRS. The antenna layout is sketched in Fig. 1. Without loss of generality, the cavity width w_1 and the cavity height h_1 were set respectively to 21 mm and 14.46 mm. The first two propagating modes in this waveguide are represented by the TE_{10} mode ($f_{cut\text{-}off}$=7.14 GHz) and the TE_{01} (f_{cut}=10.14 GHz). Because the FP leaky antenna operates with the TE_{01} mode of the waveguide, hereafter we assume that no higher-order TE modes are propagating. This clearly implies that the electric field is almost uniform along the x-axis yielding to the maximum gain condition in the xy-plane cut. The TE_{01} mode ensures the energy being radiated from the top side of the cavity once the metallic cover is replaced by a Partially Reflecting Surface (PRS). Since the TE_{10} mode is not radiating, this mode is not of interest and its excitation is undesired. The field distribution of the TE_{01} mode is nearly constant along *x*-direction and has a cosine distribution along *y*-direction.

$$E_x = \frac{\pi\omega\mu}{h_1 k_z^W}\sin\left(\frac{\pi}{h_1}y\right)e^{-jk_z^W}\,\hat{i}_x \tag{1}$$

where $k_z^W = \sqrt{k_0^2 - (\pi/h_1)^2}$ represents the propagation constant in the closed waveguide. When the top of the waveguide is replaced by the PRS, the propagation constant in the cavity becomes complex. The real part represents the modified propagation constant and the imaginary part represents the leakage rate of the cavity. The length of the antenna *L*, the PRS layout and the number of sources determine the radiation properties of the antenna.

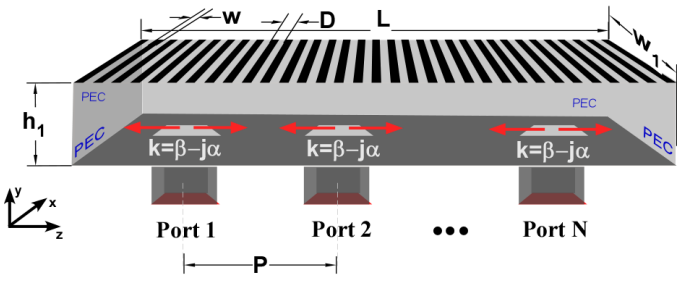

Fig. 1 – Layout of the multiple fed Fabry-Perot/leaky wave antenna.

The radiating structure can be analyzed by deriving the electric field distribution inside the cavity. The electric field distribution can be computed as the superposition of the leaky waves excited by the sources towards opposite directions. An efficient method to analyze the antenna is presented in the following two sections and the proposed approach is exploited to perform a comprehensive analysis of the antenna properties.

III. Leaky analysis of the cavity

Since the antenna radiation mechanism is based on propagating leaky waves, the first step for the analysis is to derive the propagation constant of the travelling waves. The analysis of the dispersion properties of the antenna is usually performed by using the classical Transverse Resonance Method (TRM) [2], [19], [20]. The transverse transmission line model (along *y* direction) of the antenna is shown in Fig. 2. The dispersion equation is computed by imposing the continuity of the voltages and currents at a generic interface [21], that is, the sum of input impedances looking up and down must be equal to zero:

$$Z_{down} + Z_{up} = 0 \tag{2}$$

where the impedances Z_{up} and Z_{down} are defined as:

$$Z_{down} = jZ_0^{TE}\tan\left(k_{y1}h_1\right) \tag{3}$$

$$Z_{up}^{TE} = Z_{PRS}\,//\,Z_0^{TE} \tag{4}$$

with $Z_0^{TE} = \left(\omega\mu_r\mu_0\right)/k_y$ and $k_y = \sqrt{k_0^2 - k_z^2}$.

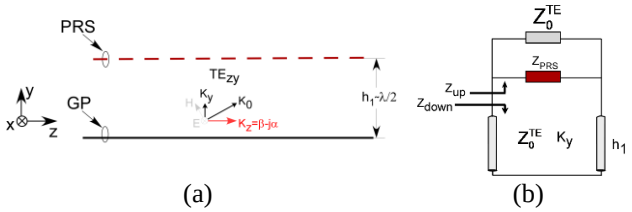

Fig. 2 – (a) Side view of the analyzed structure. (b) Transmission line model (along y direction) of the structure reported in (a).

In the present work, the PRS on the top of the cavity consists of an inductive grid. The use of such a simple FSS geometry allows using the available analytical expressions for the surface impedance. For TE polarization, the impedance of the array of strips is angle-independent and it reads [22]:

$$Z_{PRS,grid}^{TE} = j\frac{\omega\mu_0 D}{2\pi}\ln\left(\frac{1}{\sin\left(\frac{\pi w}{2D}\right)}\right) \tag{5}$$

where *D* is the grid period, *w* is the strip width and μ_0 is the free space permeability. Only TE solutions are searched for, since this is the only leaky mode excited by the slot in the ground plane. If alternative element shapes are used as the basic element of the periodic superstrate, an additional step aimed at computing the impedance of the PRS is needed [18], [19].

Equation (2) can be solved numerically by searching the zeros of the dispersion equation in the complex plane. We derived the dispersion curves starting from the solution at the highest frequency that is characterized by a low leakage rate (small attenuation). This solution is located close to the real axis and can be found by perturbing the closed waveguide solution [23]. The remaining lower frequency points are derived iteratively backward starting from the just computed frequency point.

Alternatively, by assuming that the cavity height is approximately half-wavelength [24] an analytical expression of the propagation constant can be also derived. In [24] a closed form expression for the case of a dielectric superstrate is derived. A similar approach has been used to derive a closed form expression in the case of PRS superstrate [25]:

$$k_y = \frac{\pi}{h_1} + j\frac{Z_{PRS}\left(\eta_0 - Z_{PRS}\right)}{h_1\left(\eta_0^2 - Z_{PRS}^2\right)} \tag{6}$$

In (6), h_1 represents the cavity height, Z_{PRS} is the impedance of the FSS provided in (5) and η_0 is the free space impedance, at normal incidence, computed as $\sqrt{\mu_0/\varepsilon_0}$. However, it has to be pointed out that the previous expressions have been obtained by neglecting the dependence of the free space impedance on the transversal component of the propagation constant ($Z_0^{TE} = (\omega\mu_0)/\sqrt{k_0^2 - k_z^2}$), that is, the leaky wave propagation constant k_z. We propose to retain this dependence and hence obtaining a more accurate closed form expression for k_y as a solution of the following second order equation:

$$k_y = \frac{Z_{PRS}k_y}{\mu\omega h_1 + h_1 k_y Z_{PRS}} + \frac{\pi}{h_1} \tag{7}$$

After some algebraic manipulations, the expression of the normal component of the propagation constant is derived:

$$k_y = \frac{1}{2h_1 Z_{PRS}}\Big[-\left(h_1\mu\omega - Z_{PRS}\left(\pi + j\right)\right) + \\ + \sqrt{\left(h_1\mu\omega - Z_{PRS}\left(\pi + j\right)\right)^2 + 4\pi\left(h_1 Z_{PRS}\right)\mu\omega}\Big] \tag{8}$$

The accuracy of the three solutions (TRM, relation (5) and relation (7)) is compared as a function of the PRS properties in Fig. 3. Particularly, the leaky-wave propagation constant of a cavity characterized by h_1= 14.46 mm, D= 4mm and variable w is evaluated. As evident, the proposed solution is more accurate for low reflectivity PRSs.

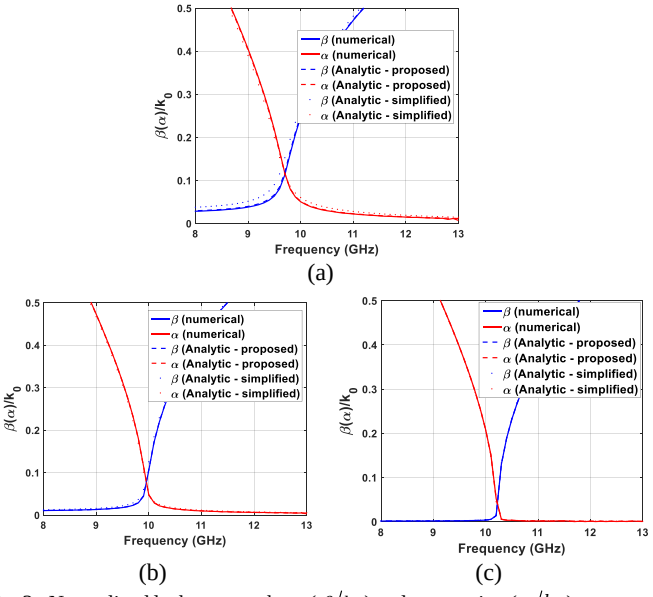

Fig. 3 - Normalized leaky-wave phase (β/k_0) and attenuation (α/k_0) constants as a function of frequency for the relevant TE leaky mode of a LWA. Proposed: relation (8), Simplified: relation (6).

The three solutions are identical for high PRS reflectivity (larger value of w). It is worth observing that the numerical approach is much more time-consuming than the analytical solution and can become unstable close to the resonance condition where the real part of the propagation constant increases in a steep way. Given the high accuracy of the analytical solution, this approach will be used for modeling the antenna hereafter. The advantage of the expression in (8) is that it represents an analytic and reliable connection between the geometrical parameters of the FSS and the complex value of the leaky propagation constant.

IV. Transmission Line Model for the Multi-Feed Leaky Antennas

Once the complex propagation constant of the leaky waves is determined through the afore presented analytical expression given in (8), the field inside the radiating structure is evaluated by using the superposition principle of the leaky waves excited by each feeder and travelling towards opposite directions. In summary, a longitudinal transmission line model (along z direction) of the structure is applied to derive the field distribution inside the cavity. Consequently, the total voltage distribution within the cavity can be written as follows:

$$V_0(z) = \sum_{n=1}^{N_{sources}} V_{in}^n e^{-jk_z\left|z - z_{source}^n\right|} \tag{9}$$

with k_z=β-$j\alpha$, V_{in}^n representing the amplitude and the phase of each feeder and z is the relative position within the cavity. The above formulation is valid under the assumption that the leaky wave is completely attenuated at the end of the cavity or an absorbing wall is placed at the end of the cavity. However, if the leaky wave is not completely attenuated at the end of the waveguide, it encounters a discontinuity and the fields are partially reflected. If the antenna is terminated with a metallic wall, the discontinuity can be efficiently modeled via the proposed transmission line approach. To this aim, two reflected waves with the same amplitude of the field but opposite phase are introduced at both sides of the cavity ($V(\pm L/2)$) to satisfy the boundary condition on a PEC wall:

$$V_1(z) = V_0(z) - V_0(L/2)e^{jk_z(z-L/2)} - V_0(-L/2)e^{-jk_z(z+L/2)} \tag{10}$$

In general, if the antenna is correctly designed, the electric field associated to the leaky wave should be almost zero close to the end of the cavity (a single reflection is sufficient to radiate all the energy). However, if the model is used also above the splitting condition of the cavity [2] (when α becomes smaller than β), where the attenuation constant of the leaky wave is very low, the reflection condition at the end of the cavity has to be applied iteratively for a number of bounces $P_{bounces}$ in order to get the field approaching 0 at $z = \pm L/2$.

$$V_p(z) = V_{p-1}(z) - V_{p-1}(L/2)e^{jk_z(z-L/2)} + \\ - V_{p-1}(-L/2)e^{-jk_z(z+L/2)} \tag{11}$$

Once that the propagating waves are summed coherently and the total electric field distribution inside the cavity is derived, the radiation pattern $P(\theta)$ of the antenna can be computed by performing the Fast Fourier Transform (FFT) [26]:

$$P(\theta)=\cos(\theta)\sum_{m=-M}^{M}V(m)e^{jk\cdot m\cdot\Delta z\cdot\sin(\theta)} \quad (12)$$

where m represents the m^{th} sample of the voltage inside the cavity and Δz is the spatial sampling of the field distribution on the cavity (L=(2M+1)Δz). The term $cos(\theta)$, according to Tamir and Oliner paper [27], ensures that the field goes to zero at $\theta=\pm 90°$. The knowledge of the field distribution inside the cavity is important to evaluate the performance of the antenna in terms of aperture illumination efficiency. The illumination efficiency is computed as follows:

$$\eta_{\%}=\frac{1}{L}\frac{\left(\int_{-L/2}^{L/2}\left|V(z_s)\right|dz\right)^2}{\int_{-L/2}^{L/2}\left|V(z_s)\right|^2 dz} \quad (13)$$

where L is the total length of the cavity. The integral is solved numerically by discretizing the aperture interval L with the spatial sampling Δz. According to the theory of aperture antennas, if the illumination efficiency approaches 100%, the maximum possible gain is obtained for a certain dimension of the cavity. As previously remarked, the design of a very large aperture Fabry-Perot configuration, by employing only one single source, is a challenging task since the typical strategy to improve the illumination efficiency is to decrease the leakage rate of the leaky wave, that is, to increase the reflectivity of the partially reflective surface. In our case, the reflectivity can be increased by simply enlarging the strip width while keeping fixed the FSS periodicity. However, an indiscriminate increase of the FSS reflectivity brings to a high Q cavity which implies a strong bandwidth reduction, complicate matching of the feeder and issues with full-wave numerical simulations. The limiting case is represented by the metallic top layer as in [28], where the radiation is obtained only from the edges of the antenna. The use of the TL model allows an instantaneous prediction of the antenna radiation pattern.

V. TL Model Verification

The effect of using single or multiple sources will be analyzed for a benchmark antenna configuration characterized by a total length of 30 cm and a width of 3 cm. The aperture is roughly 10 wavelengths at 10 GHz. The aperture is not extremely large but it is sufficient to analyze the multi-source configuration advantages and, at the same time, verify the accuracy of the proposed transmission line model against the full-wave results obtained by Ansys Electronics v.16 [29]. The parameters of the PRS are the following: periodicity D equal to 4 mm and strip width w ranging from 0.5 to 1 mm. Initially, the behavior of the Fabry-Perot antenna fed by a single source as a function of frequency is computed. It is evident that the use of a 1-mm strip width (w) allows to illuminate the cavity more efficiently than w=0.5 mm. The maximum directivity is also higher with respect to the one achieved by using narrower strips, but this is paid in terms of bandwidth and matching of the feed. This is confirmed by analyzing the antenna through full-wave simulations. In Fig. 4 the maximum directivity computed by Ansys and by the TL model are reported as a function of the strip width. The maximum gain operating bandwidth depends on the strip width according to the leaky-wave propagation constant (see Fig. 3). The s_{11} of the antenna is also reported on the same plot. It is worth underlining that, in general, matching a Fabry-Perot antenna employing a high reflectivity superstrate is a difficult task.

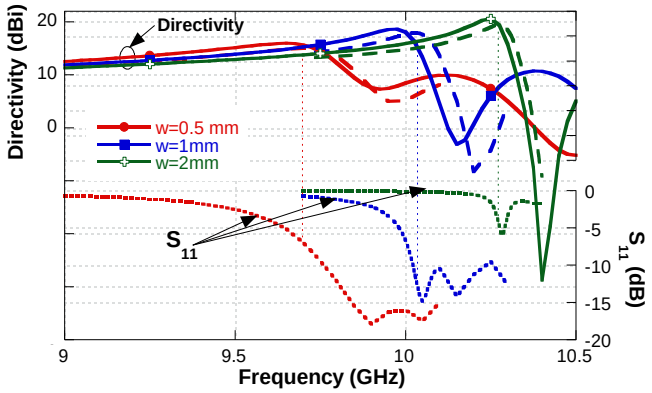

Fig. 4 – Maximum boresight directivity of the antenna feed with a single source and the s_{11} of the antenna for three different values of the strip width (w=0.5 mm, w=1 mm, w=2 mm). Continuous line: Transmission line approach, dashed lines: Ansys Electronics.

On the contrary, if multiple sources are employed to illuminate the whole cavity, a good illumination efficiency can be achieved also by using a low reflectivity superstrate (narrow strips). This allows obtaining a high maximum directivity and hence a high illumination efficiency, while preserving at the same time, a reasonable bandwidth and a good impedance matching. An example of the field distribution inside the cavity obtained with a single source and with three sources, by keeping constant the FSS reflectivity (w=0.5 mm) is shown in Fig. 5. It is evident that, in the case of a single source, the choice of w=0.5 mm does not allow to illuminate entirely the cavity. Differently, the use of 3 sources is sufficient to properly illuminate the cavity.

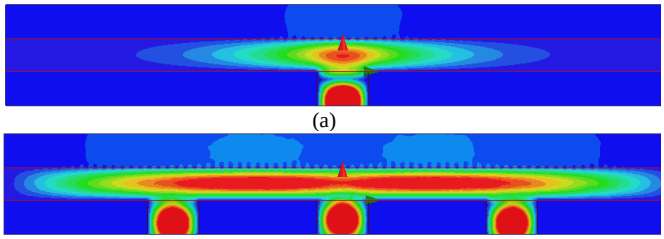

(a)

(b)

Fig. 5 – Color plot of the electric field distribution inside the Fabry-Perot cavity on H-plane (yz plane) for the case of single source and three sources cavity with w=1 mm. (a) single source f=9.9 GHz, (b) 3 sources , f=10 GHz.

In order to verify the accuracy of the TL model predictions, the radiation pattern and field distributions of the antenna fed by three sources are computed by using the TL model and the full-wave approach (HFSS - Ansys Electronics simulations). The patterns and the field distribution are reported for three different values of the strip width (w=0.5 mm and w=1mm) at different frequencies inside the operating bandwidth in Fig. 6 and Fig. 7. It is apparent that the field distributions of TL approach agree very well with full-wave simulations.

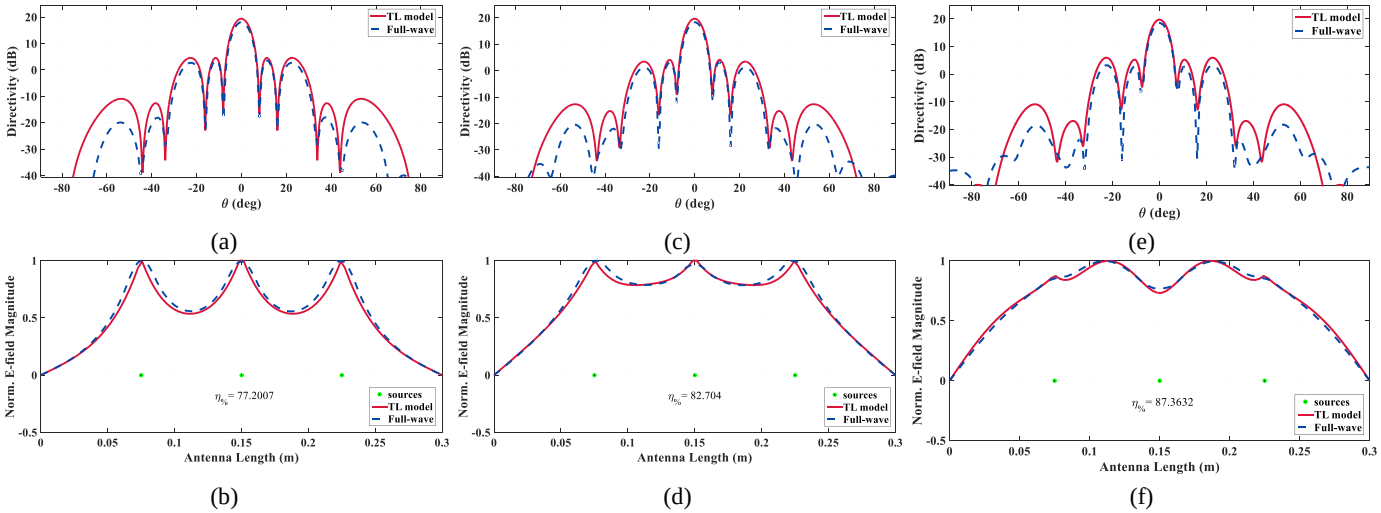

Fig. 6 - Radiation pattern on the zy plane computed with the model and by using the full-wave approach: (a) 9.6 GHz, (c) 9.7 GHz (e) 9.8 GHz. Electric field distribution inside the Fabry-Perot cavity computed by using the transmission line model and the full-wave approach. (b) 9.6 GHz, (d) 9.7 GHz (f) 9.8 GHz. FSS Parameters: D=4 mm, w=0.5 mm.

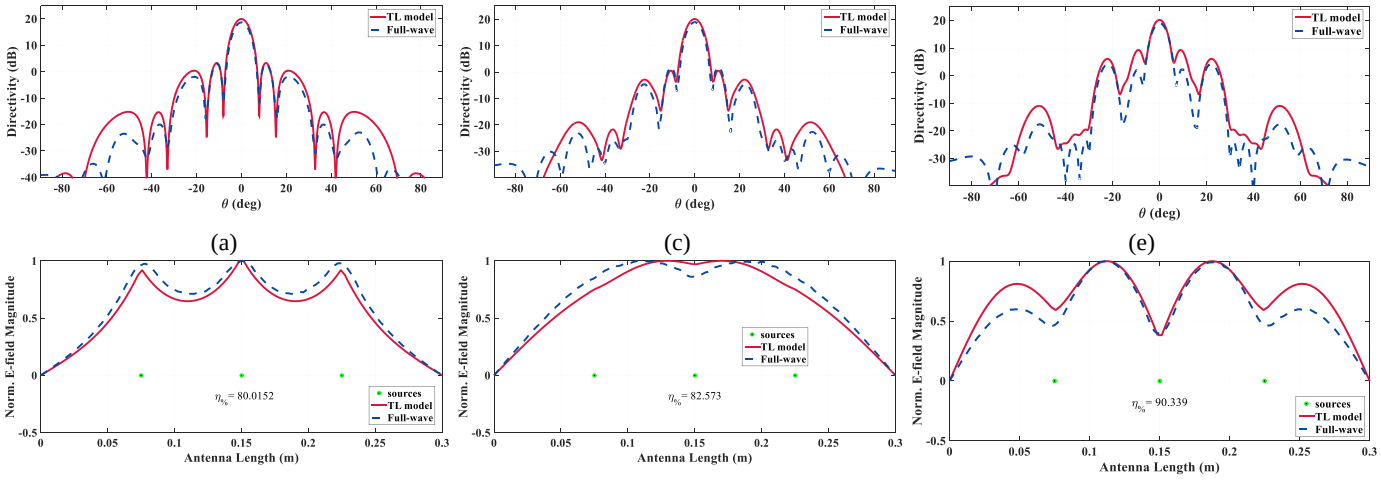

Fig. 7 - Radiation pattern on the zy plane computed with the model and by using the full-wave approach: (a) 9.9 GHz, (c) 10 GHz (e) 10.1 GHz. Electric field distribution inside the Fabry-Perot cavity computed by using the transmission line model and the full-wave approach. (b) 9.9 GHz, (d) 10 GHz (f) 10.1 GHz. FSS Parameters: D=4 mm, w=1 mm.

The value of the aperture efficiency obtained by using relation (13) is reported inside the plot of the electric field distribution. In all cases, when the field distribution tends to split in the middle of the aperture, an increase of the sidelobe level is observed. The pattern estimation is very accurate up to ± 40 degrees. It is interesting noting that in the case of three sources, even if the aperture is quasi-uniformly illuminated, setting w=2 mm would let the feeders to interact strongly with each other thus producing an extremely overlapped field distribution. Therefore, this design choice would create issues in terms of coupling between adjacent ports and furthermore would not help to improve the antenna bandwidth [30].

VI. Optimal Number of Sources

As demonstrated in the previous examples the use of multiple sources allows obtaining better illumination efficiency and a higher gain/bandwidth product with respect to the single-source feeding technique. However, the appropriate number of sources for a given aperture size must be adequately chosen. To this aim, it is desirable minimizing the number of employed sources without compromising the shape of the radiation patterns. The number of sources needs to be minimized also for avoiding mutual coupling effects among the sources that share a common cavity [30]. For this reason, in the next paragraph we analyze the main parameters that regulates the choice of the suitable number of sources in the case of an aperture of length 30 cm.

a) Number of feeds (overlapping)

Let us assume to illuminate the same cavity (30 cm × 3 cm) with three equally spaced sources but with different properties of the PRS cover. Increasing the width of the strips, while keeping the PRS periodicity fixed at 4 mm, leads to an increased reflectivity and thus to a larger spreading of the field around every source. This means that a certain overlapping of the field is achieved inside the cavity. As the overlapping is increased, a higher coupling between closely located ports can be expected [30]. Indeed, as it is shown in Fig. 8, the coupling coefficients increase if the width of the strips is enlarged. On the contrary, decreasing the width of the strips allows obtaining a reasonable matching even when all sources are fed. Once the best

configuration in terms of radiation pattern is chosen, a number of strategies can be adopted to improve the antennas matching. For instance, the slot shape can be adequately chosen [31], [32] or a gradually tapered transition between a standard waveguide and a narrow slot can be adopted [33].

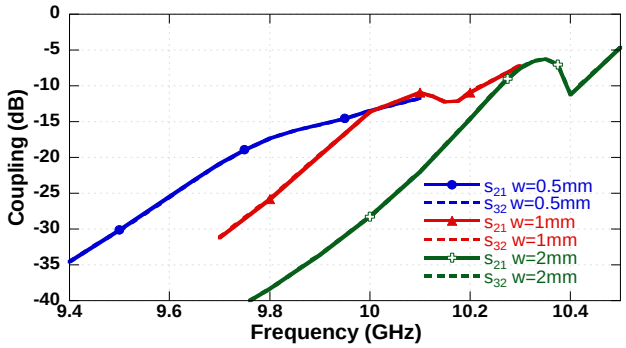

Fig. 8 – Coupling coefficients (s_{21} and s_{32}) of the ports for different width of the periodic strips forming the top layer of the cavity.

b) Bandwidth properties

One of the most interesting property achieved by increasing the number of sources is the antenna bandwidth improvement. As previously remarked, a very large aperture illuminated with a single source would lead to a very narrowband configuration since a very high reflectivity superstrate needs to be selected. Conversely, using multiple sources allows operating with moderately low-reflective superstrates.

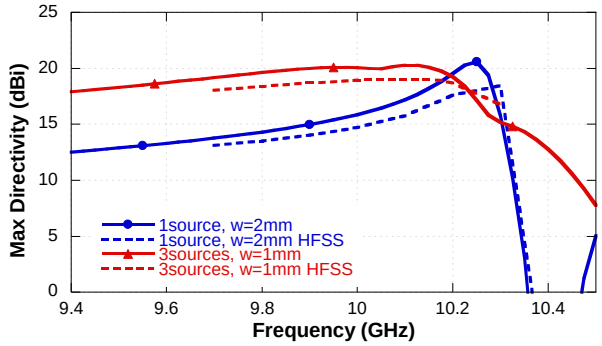

Fig. 9 – Peak boresight gain by using the single source feed and *w*=2mm and by employing three sources with *w*=1mm. Cavity size is 30 cm × 3 cm.

Fig. 9 shows the maximum boresight gain achieved when a single source with strip width of 2 mm or three sources with a strip width of 1 mm are used.

As it is apparent, a much larger bandwidth is obtained when three sources are used, and a similar level of peak gain is guaranteed. The same also holds for the impedance bandwidth. Remarkably, the results obtained with full-wave simulations are again in a good agreement with the transmission line approach.

c) Scan properties

The antenna excited with multiple sources can be interpreted as a thinned linear array of directive subarrays [16]. In the analyzed example, a 30-cm aperture is illuminated by three equally spaced sourcs with inter-element distance of 75 mm (about 2.5 wavelength at 10 GHz). According to the array theory, changing progressively the phases of the sources allows to scan the main beam over a limited-field-of-view (LFOV) sector. The scanning is limited since the half-power beamwidth (HPBW) of the radiation pattern of the isolated element, that is, the single-fed cavity, is narrow. An idealized sketch useful to represent the maximum scan range of the antenna is illustrated in Fig. 10. It is evident that the larger is the aperture size of the single element (*L* in this case) the more directive is the element pattern. The grating lobes replica can be found at λ/P, where *P* is the spacing between two adjacent ports. The maximum scanning range of the array antenna is determined by the HPBW of the element pattern.

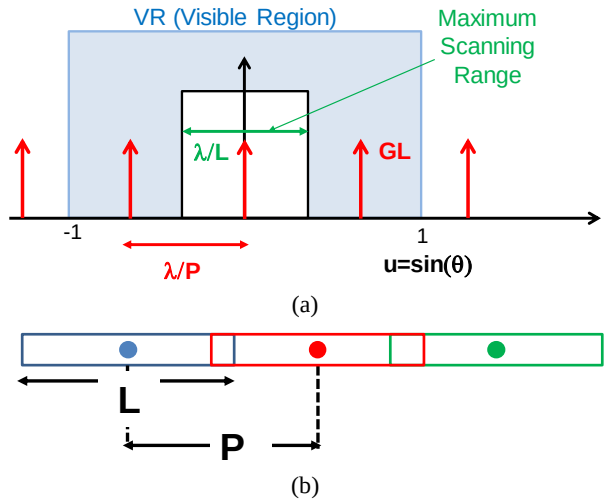

Fig. 10 – Idealized representation of the array factor quantization lobes (red arrows) and element factor mainlobe (light region) within the visible space.

An example of main beam steering is plotted in Fig. 11 where a progressive phase shift φ of 30° or 60° is applied between two consecutive input ports. In this case, the strip width is equal to 0.5 mm and the results are plotted at 9.7 GHz. The expected scanning angle is given by the following relation:

$$\theta = \sin^{-1}\left(\varphi / \beta P\right) \tag{14}$$

The actual pointing angle is slightly shifted with respect to the expected one, since the element pattern is clearly not flat-topped over the whole scan range [34] and differs from feeder to feeder due to the cavity truncation effects.

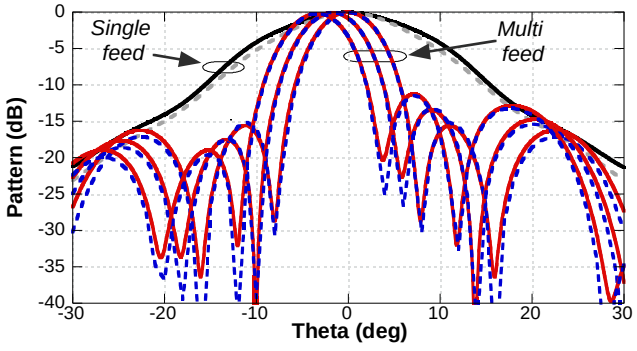

Fig. 11 – Radiation pattern of a three-element feed Fabry-Perot cavity for a phase displacement among two consecutive ports of 30° or 60°. The Radiation pattern of the single feed Fabry-Perot cavity with the same parameters and at the same frequency is reported for comparison. Continuous line: TL model, dashed lines: Full-wave code.

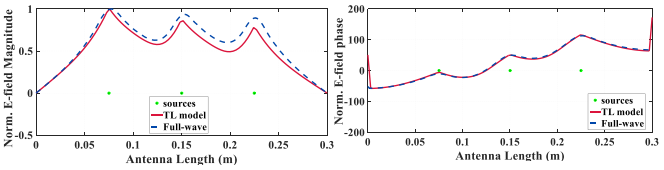

(a) (b)

Fig. 12 - Electric field distribution inside the Fabry-Perot cavity computed by using the transmission line model and the full-wave approach. (a) Amplitude for ΔΦ=60°, (b) Phase for ΔΦ=60°.

An additional interesting aspect is that the scan losses of the multi-fed cavity are lower than expected if one looks at the element pattern, *i.e.* the isolated center-fed cavity. This is mainly due to the fact that a part of the field is reflected back at the end of the cavity because of the presence of the metallic walls. This effect is clearly accounted for in the model by short-circuiting the equivalent longitudinal TL model at the extremes. The amplitude and the phase of the electric field distribution inside the cavity is reported in FIG. 12. The behavior obtained by using the TL model agrees well with the full-wave HFSS results.

VII. LARGE APERTURE DESIGN

The previously presented results are related to a 30-cm long cavity antenna excited by three ports. Since the HFSS analysis of highly resonant structures poses a crucial issue of computational burden, the antenna electric length has been kept below 10 wavelengths for reason of results comparison. Once the model accuracy has been verified, the TL approach can also be employed for designing a larger aperture Fabry-Perot antenna with a narrower beamwidth and hence a higher gain. As an example, a 90 cm long antenna has been analyzed. Since the full-wave simulation of this structure is not feasible due to the computational burden involved, only the TL model results are provided in this case. The electric field distribution and radiation pattern of the antenna as a function of both the number of sources and the FSS strip reflectivity are reported in Fig. 13. As expected, by increasing the strip width, a better illumination of the aperture is achieved with a single feed.

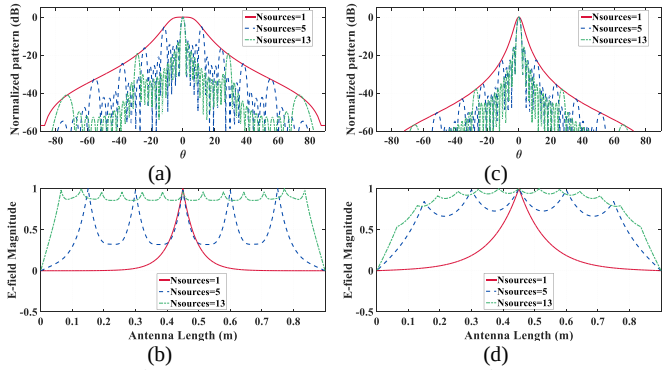

(a) (c)
(b) (d)

Fig. 13 - Electric field distribution and radiation patterns of a 0.9 m long Fabry-Perot cavity computed by using the transmission line model with a variable number of sources. Simulations are performed also a function of the FSS reflectivity (a,b) w=0.5 mm and f=9.7 GHz (c,d) w=2 mm and f=10.2 GHz.

However, when multiple sources are employed, even the use of a low-reflectivity FSS allows obtaining a directive beam with a controlled sidelobe level. Moreover, it is worthwhile noting that, if we fix the number of sources, the grating lobe rejection increases as the FSS reflectivity approaches the unity. However, it is important to point out that employing a low-reflectivity FSS results in a smaller mutual coupling and a wider operating bandwidth both in terms of impedance matching and maximum gain. A low reflectivity superstrate makes also the antenna prototype more robust to fabrication tolerances. To summarize, given a certain aperture of the antenna, the number of sources should be traded off for the FSS reflectivity (here controlled by changing the *w* parameter) with the aim of keeping this latter as small as possible. An alternative strategy to reduce the sidelobe level is to use non-uniformly spaced sources [11].

VIII. EXPERIMENTAL REALIZATION

A prototype of the antenna with three sources has been fabricated to experimentally verify the performance. The antenna has been fabricated by using the 3D aluminum printing process. The front view of the 3D model of the fabricated antenna is shown in Fig. 14. The antenna is fed through three standard WR90 waveguides. With the aim of matching the antenna input ports, an optimized pyramidal waveguide-to-slot transition has been designed.

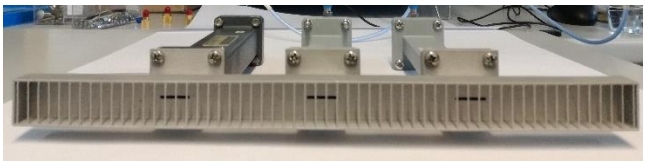

Fig. 14 – Prototype of the Fabry-Perot cavity fed with three waveguides.

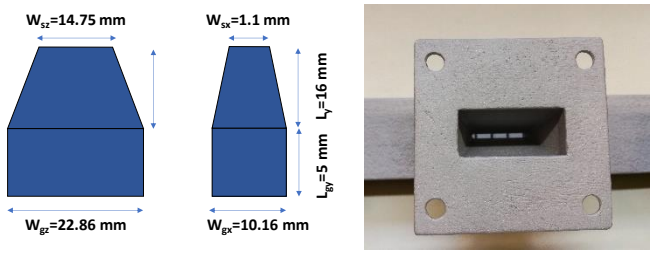

(a) (b)

Fig. 15 – (a) Parameters of the waveguide-to-slot transition used to feed the antenna and (b) the detailed view of the waveguide transition fabricated with the 3D aluminum printing process.

The parameters of the optimized transition and a close-up view of the feeding section are shown in Fig. 15. In order to fulfill the tolerances of the manufacturing process and account for the effects of the wall thickness, the FSS superstrate parameters have been modified as D=5.4 mm and w=0.5 mm. The resulting total length of the antenna is 301 mm. The antenna has been characterized both in terms of scattering parameters and radiation properties. The measurements have been also compared with the results predicted by HFSS and the TL model here introduced for the performance assessment analysis. The active S parameters of the center port and the edge port are reported in Fig. 16, when all the elements are uniformly in-phase excited. The broadside gain of the antenna is also superimposed thus highlighting the operating frequency of the cavity which is approximately around 10.2 GHz. It is evident that both the measured directivity and active scattering parameters as a

function of frequency show a good agreement with the computed results.

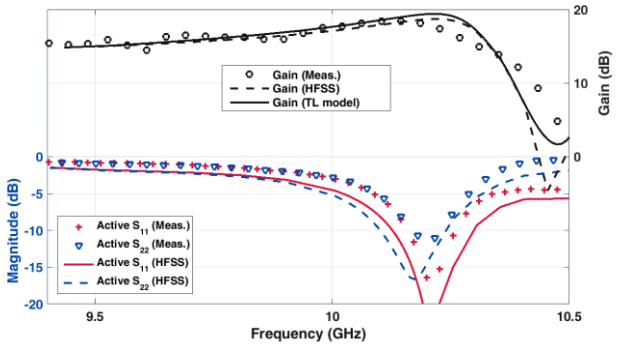

Fig. 16 – Active S parameters of the antenna input ports (center port and one of the edge port) and the broadside gain as a function of the frequency

With the aim of analyzing the radiation pattern of the antenna when the main beam is scanned, the array pattern is evaluated by applying the following formulation:

$$AP(\theta) = \sum_{i_{elem}=1}^{3} V_{i_{elem}}^{Tot}(\theta_{\max}) EP_{i_{elem}}(\theta) e^{jkP(i_{elem}-1)\sin\theta} \qquad (15)$$

In (15), the array pattern *AP* is given as a weighted sum of the embedded element radiation pattern *EP* of each i_{elem}-th port. The other parameters *k*, P and $\theta_{\max}$ represent respectively the wavenumber, the interelement spacing and the desired angle of maximum radiation. It is worth evidencing that the mutual coupling effect among the ports has been taken into account by modifying the incident complex excitation vector $\underline{V}^{+}$ into $\underline{V}^{Tot}$ according to the following relation [35]:

$$\underline{V}^{Tot}(\theta_{\max}) = \left(\underline{\underline{I}} + \underline{\underline{S}}\right)\underline{V}^{+}(\theta_{\max}) \qquad (16)$$

where $\underline{\underline{I}}$ and $\underline{\underline{S}}$ are respectively the identity matrix and the scattering matrix.

The embedded element pattern which is defined as the radiation pattern when only the port under consideration is fed and the remaining ones are matched terminated, are plotted in Fig. 17 for the center port (Port 2) and the edge port (Port 1). It is apparent that the simulated results with HFSS are in a good agreement with the measurements as long as the magnitudes are within the threshold of 30 dB below the main beam.

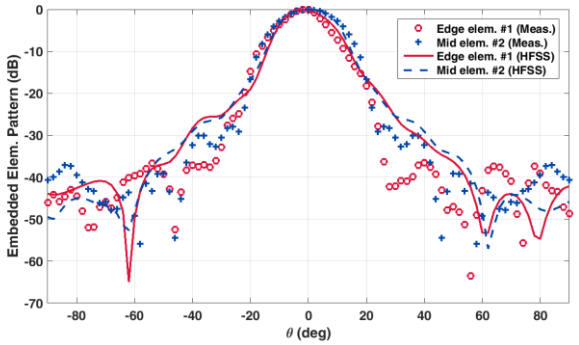

Fig. 17 – Measured embedded element radiation pattern of the center port (Port 2) and the edge port (Port 1). The radiation patterns are evaluated at 10.19 GHz.

Beyond this limit, the measurements were affected by several limitations, mainly due to the errors of the positioning system and the presence of a noisy measurement environment that was not totally reflection-free. The same consideration also applies to the measured array pattern shown below. The superimposition of the measured array pattern with those predicted by the TL model and HFSS is reported in Fig. 18 and Fig. 19, respectively when the main beam is steered at broadside and 4° off broadside. Again, the results estimated by the TL model well match those of HFSS and this is further confirmed by the measurements.

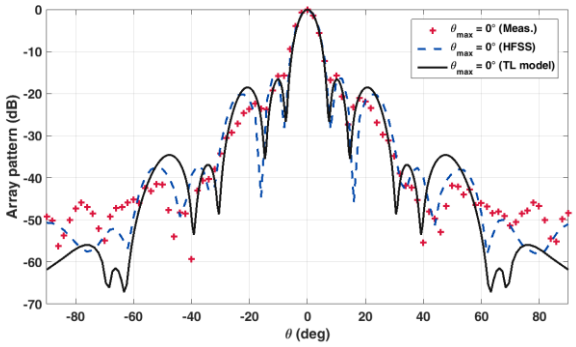

Fig. 18 – Main beam steering of the fully active cavity antenna at broadside. The radiation patterns are evaluated at 10.19 GHz.

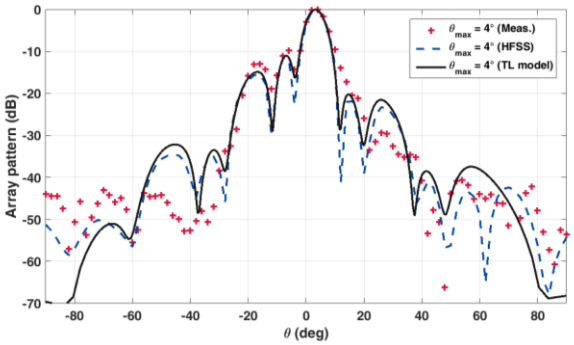

Fig. 19 - Main beam steering of the fully active cavity antenna at 4° off broadside. The radiation patterns are evaluated at 10.19 GHz.

IX. Conclusions

A comprehensive analysis of linear Fabry-Perot antennas excited by multiple sources has been presented. The properties of the multi-fed antenna and its advantages with respect to the single-fed configuration are discussed. The analysis is performed by using two equivalent transmission line models: the first one (toward transversal direction) is used to compute analytically the propagation constant of the leaky waves travelling inside the cavity and the second one (toward longitudinal direction) is used to compute the field distribution inside the cavity. A novel fully analytic expression for the propagation constant is proposed, which agrees very well with numerical solution of the dispersion equation. The radiation pattern is finally computed via the Fast Fourier Transform. The results obtained through the TL approach have been methodically compared against full-wave Finite Element Method (FEM) simulations demonstrating the high accuracy of the proposed method. The proposed approach has been then employed to draw guidelines for designing very large aperture and high gain antennas where a full-wave approach is not feasible. A prototype of the cavity antenna fed with three waveguides has been fabricated by using the 3D aluminum printing process and measured.

X. REFERENCES

[1] D. R. Jackson, C. Caloz, and T. Itoh, "Leaky-Wave Antennas," *Proceedings of the IEEE*, vol. 100, no. 7, pp. 2194–2206, Jul. 2012.

[2] G. Lovat, P. Burghignoli, and D. R. Jackson, "Fundamental properties and optimization of broadside radiation from uniform leaky-wave antennas," *IEEE Transactions on Antennas and Propagation*, vol. 54, no. 5, pp. 1442–1452, May 2006.

[3] G. V. Trentini, "Partially reflecting sheet arrays," *IRE Transactions on Antennas and Propagation*, vol. 4, no. 4, pp. 666–671, Oct. 1956.

[4] A. P. Feresidis, G. Goussetis, S. Wang, and J. C. Vardaxoglou, "Artificial magnetic conductor surfaces and their application to low-profile high-gain planar antennas," *IEEE Transactions on Antennas and Propagation*, vol. 53, no. 1, pp. 209–215, Jan. 2005.

[5] F. Costa and A. Monorchio, "Design of subwavelength tunable and steerable fabry-perot/leaky wave antennas," *Progress In Electromagnetics Research*, vol. 111, pp. 467–481, 2011.

[6] R. Sauleau, "Fabry–Perot Resonators," in *Encyclopedia of RF and Microwave Engineering*, John Wiley & Sons, Inc., 2005.

[7] A. P. Feresidis and J. C. Vardaxoglou, "A broadband high-gain resonant cavity antenna with single feed," in *First European Conference on Antennas and Propagation, 2006. EuCAP 2006*, 2006, pp. 1–5.

[8] Y.-F. Lu and Y.-C. Lin, "Design and implementation of broadband partially reflective surface antenna," in *2011 IEEE International Symposium on Antennas and Propagation (APSURSI)*, 2011, pp. 2250–2253.

[9] K. F. Warnick and B. D. Jeffs, "Gain and Aperture Efficiency for a Reflector Antenna With an Array Feed," *IEEE Antennas and Wireless Propagation Letters*, vol. 5, no. 1, pp. 499–502, Dec. 2006.

[10] R. Gardelli, M. Albani, and F. Capolino, "Array thinning by using antennas in a Fabry-Perot cavity for gain enhancement," *IEEE Transactions on Antennas and Propagation*, vol. 54, no. 7, pp. 1979–1990, Jul. 2006.

[11] F. Capolino, M. Albani, and V. Galdi, "Array thinning with periodic and aperiodic distributions in a Fabry-Perot Cavity for gain enhancement," in *IEEE Antennas and Propagation Society International Symposium, 2008. AP-S 2008*, 2008, pp. 1–4.

[12] J. Kim, M.-G. Kim, and R. Mittra, "Scan capability of fabry perot cavity (FPC) antennas with array feeds," in *2012 IEEE Antennas and Propagation Society International Symposium (APSURSI)*, 2012, pp. 1–2.

[13] F. Scattone, M. Ettorre, B. Fuchs, R. Sauleau, and N. J. G. Fonseca, "Synthesis procedure for thinned leaky-wave phased array antennas," in *2015 9th European Conference on Antennas and Propagation (EuCAP)*, 2015, pp. 1–4.

[14] M. Hajj *et al.*, "Design of Sectoral Antennas Using a Metallic EBG Structure and Multiple Sources Feeding for Base Station Applications," *International Journal of Antennas and Propagation*, vol. 2008, p. e359053, Feb. 2009.

[15] S. Kabiri, S. Ali Hosseini, F. Capolino, and F. De Flaviis, "Gain-bandwidth enhancement of 60GHz single-layer Fabry-Perot cavity antennas using sparse-array," in *2014 IEEE Antennas and Propagation Society International Symposium (APSURSI)*, 2014, pp. 739–740.

[16] N. Llombart, D. Blanco, E. Rajo-Iglesias, J. Campuzano, and A. Montesano-Benito, "Leaky wave enhanced phased array for the reduction of the grating lobe level," in *2012 IEEE Antennas and Propagation Society International Symposium (APSURSI)*, 2012, pp. 1–2.

[17] B. A. Munk, *Frequency Selective Surfaces: Theory and Design*. John Wiley & Sons, 2005.

[18] F. Costa, A. Monorchio, and G. Manara, "An Overview of Equivalent Circuit Modeling Techniques of Frequency Selective Surfaces and Metasurfaces.," *Applied Computational Electromagnetics Society Journal*, vol. 29, no. 12, 2014.

[19] M. G. Vigueras, J. L. G. Tornero, G. Goussetis, and A. A. Melcon, "Software tool for the leaky-mode analysis of waveguides loaded with frequency selective surfaces," in *3rd European Conference on Antennas and Propagation, 2009. EuCAP 2009*, 2009, pp. 83–87.

[20] F. Costa, D. Bianchi, A. Monorchio, and G. Manara, "Efficient design of multiple-fed leaky wave/Fabry-Perot antennas," in *2016 IEEE International Symposium on Antennas and Propagation (APSURSI)*, 2016, pp. 543–544.

[21] N. Marcuvitz, *Waveguide handbook*. Iet, 1951.

[22] O. Luukkonen *et al.*, "Simple and Accurate Analytical Model of Planar Grids and High-Impedance Surfaces Comprising Metal Strips or Patches," *IEEE Transactions on Antennas and Propagation*, vol. 56, no. 6, pp. 1624–1632, Jun. 2008.

[23] M. G. Vigueras, J. L. G. Tornero, G. Goussetis, and A. A. Melcon, "Software tool for the leaky-mode analysis of waveguides loaded with frequency selective surfaces," in *3rd European Conference on Antennas and Propagation, 2009. EuCAP 2009*, 2009, pp. 83–87.

[24] A. Neto and N. Llombart, "Wideband Localization of the Dominant Leaky Wave Poles in Dielectric Covered Antennas," *IEEE Antennas and Wireless Propagation Letters*, vol. 5, no. 1, pp. 549–551, Dec. 2006.

[25] M. Ettorre, "Analysis and design of efficient planar leaky-wave antennas," Universita Degli Studi di Siena, 2008.

[26] K. Dutta, D. Guha, and C. Kumar, "Theory of Controlled Aperture Field for Advanced Superstrate Design of a Resonance Cavity Antenna With Improved Radiations Properties," *IEEE Transactions on Antennas and Propagation*, vol. 65, no. 3, pp. 1399–1403, Mar. 2017.

[27] T. Tamir and A. A. Oliner, "Guided complex waves. Part 2: Relation to radiation patterns," *Proceedings of the Institution of Electrical Engineers*, vol. 110, no. 2, pp. 325–334, Feb. 1963.

[28] K. Dutta, D. Guha, C. Kumar, and Y. M. M. Antar, "New Approach in Designing Resonance Cavity High-Gain Antenna Using Nontransparent Conducting Sheet as the Superstrate," *IEEE Transactions on Antennas and Propagation*, vol. 63, no. 6, pp. 2807–2813, Jun. 2015.

[29] "Ansys HSS ver 16." [Online]. Available: http://www.ansys.com/products/electronics.

[30] N. Llombart, A. Neto, G. Gerini, M. Bonnedal, and P. D. Maagt, "Impact of Mutual Coupling in Leaky Wave Enhanced Imaging Arrays," *IEEE Transactions on Antennas and Propagation*, vol. 56, no. 4, pp. 1201–1206, Apr. 2008.

[31] J. R. Kelly, T. Kokkinos, and A. P. Feresidis, "Analysis and Design of Sub-Wavelength Resonant Cavity Type 2-D Leaky-Wave Antennas," *IEEE Transactions on Antennas and Propagation*, vol. 56, no. 9, pp. 2817–2825, Sep. 2008.

[32] N. Llombart, A. Neto, G. Gerini, M. Bonnedal, and P. D. Maagt, "Leaky wave enhanced feed arrays for the improvement of the edge of coverage gain in multibeam reflector antennas," *IEEE Transactions on Antennas and Propagation*, vol. 56, no. 5, pp. 1280–1291, Maggio 2008.

[33] G. D. Massa, S. Costanzo, and H. O. Moreno, "Planar Fabry–Perot directive antenna: a simplified analysis by equivalent circuit approach," *Journal of Electromagnetic Waves and Applications*, vol. 29, no. 2, pp. 261–274, Jan. 2015.

[34] R. J. Mailloux, *Phased array antenna handbook*, vol. 2. Artech House Boston, 2005.

[35] L. Josefsson and P. Persson, *Conformal Array Antenna Theory and Design*, pp. 411-412, John Wiley & Sons, 2006.

Filippo Costa (S'07-M'11) received the M.Sc. degree in telecommunication engineering and the Ph.D. degree in applied electromagnetism from the University of Pisa, Pisa, Italy, in 2006 and 2010, respectively. In 2009, he was a Visiting Researcher at the Department of Radio Science and Engineering, Helsinki University of Technology, TKK (now Aalto University), Finland.

He is currently an Assistant Professor at the University of Pisa. His research interests include metamaterials, metasurfaces, antennas and Radio Frequency Identification (RFID).

He was appointed several times as outstanding reviewer of IEEE TRANSACTIONS ON ANTENNAS AND PROPAGATION and IEEE ANTENNAS AND WIRELESS PROPAGATION LETTERS. He received three times the URSI Young Scientist Award in 2013, 2014 and 2015. He serves as an Associate Editor of the IEEE SENSORS LETTERS.

Davide Bianchi (S'13-M'17) was born in Livorno, Tuscany, IT, in 1983. He received the B.S. and M.S. degrees in Telecommunication engineering from The University of Pisa, IT, in 2006 and 2008, respectively. After being the recipient of a grant issued by the italian Ministry of Education and Science (MIUR), in 2013 he receiveid the Ph.D. degree in remote sensing engineering at the Pisa University Department of Information Engineering. Since 2009 Mr. Bianchi has been affiliated with the National InterUniversity Consortium for Telecommunications (CNIT) which presented him with a research grant in the field of antenna theory and design for HF-Skywave radar applications. In 2010 he was presented with a 2009-2010 FSE (European Social Fund) Graduate Student Award and he was a visiting student in the Pennsylvania State University (Penn State) at the Computational Electromagnetics and Antennas Research Lab (CEARL), University Park. Since 2012 he has been affiliated with the National Laboratory Radar and Surveillance (RaSS) and he is currently a Postdoctoral Research Fellow for the Microwave and Radiation Lab (MRL) at the University of Pisa. His main research topics include computational electromagnetics and evolutionary strategies with applications to ultrawideband and phased array design as well as conformal antenna optimization and miniaturization. Other interests include parallel and high performance computer programming.

Agostino Monorchio (S'89–M'96–SM'04–F'12), Professor at the Department of Information Engineering of the University of Pisa, is active in a number of areas related to electromagnetics, including computational numerical techniques, microwave metamaterials, radio propagation for wireless systems, the design and miniaturization of antennas and electromagnetic compatibility, microwaves biomedical applications.

Giuliano Manara received the Laurea (Doctor) degree in electronics engineering (summa cum laude) from the University of Florence, Italy, in 1979. Currently, he is a Professor of the University of Pisa, Italy. From 2000 to 2010 and since 2013, he has been serving as the President of the Bachelor and the Master Programs in Telecommunications Engineering at the same University. Since 2010, he has been serving as the President of the Bachelor Program in Telecommunications Engineering at the Italian Navy Accademy in Livorno, Italy. Since 1980, he has been collaborating with the Department of Electrical Engineering of the Ohio State University, Columbus, Ohio, USA, where, in the summer and fall of 1987, he was involved in research at the ElectroScience Laboratory.

His research interests have centered mainly on the asymptotic solution of radiation and scattering problems. He has also been engaged in research on numerical, analytical and hybrid techniques, frequency selective surfaces (FSS) and electromagnetic compatibility. More recently, his research has also been focused on antenna design and on Radio Frequency Identification (RFID).

Prof. Manara was elected an IEEE (Institute of Electrical and Electronic Engineers) Fellow in 2004 for "contributions to the uniform geometrical theory of diffraction and its applications.". He served as the International Chair of URSI Commission B for the triennium 2011-2014. Prof. Manara has served as the General Chair of the International Symposium on Electromagnetic Theory (EMTS 2013), held in Hiroshima, Japan, May 20-24, 2013.

Prof. Manara is the President of CUBIT (Consortium UBIquitous Technologies) S.C.A.R.L., a consortium created by the Dipartimento di Ingegneria dell'Informazione of the University of Pisa, Polo Navacchio S.p.A. (Navacchio, Cascina) and some highly innovative Italian companies, with the aim of defining a new knowledge transfer model from university to industry.